




Structural evolution, Raman spectra, and microwave dielectric properties of Zr-substituted $\text{ZnTiTa}_2\text{O}_8$ ceramics

Shiyuan Wang¹ · Boyuan Xiao¹ · Jiayi Li¹ · Yifan Li¹ · Liezheng Lv¹ · Guangfan Tan¹ · Yingchun Zhang¹ 

Received: 29 March 2020 / Accepted: 8 May 2020 / Published online: 16 May 2020
© Springer Science+Business Media, LLC, part of Springer Nature 2020

Abstract

A series of $\text{Zn}(\text{Ti}_{1-x}\text{Zr}_x)\text{Ta}_2\text{O}_8$ ($x = 0, 0.2, 0.4, 0.6, 0.8, 1$) ceramics samples were synthesized by conventional solid-state reaction route. The sintering behavior, crystal structure, Raman spectroscopy, microstructure, and microwave dielectric properties were studied. The crystal structure, lattice parameters, and bonding of the ceramics were analyzed using X-ray powder diffraction and Raman spectroscopy. As Zr^{4+} content increasing, the structural transition followed the sequence: tri-rutile \rightarrow coexistence of tri-rutile and columbite \rightarrow columbite \rightarrow wolframite. The microwave dielectric properties of ceramics were considerably affected by the structural transition. Compared with pure phase $\text{ZnTiTa}_2\text{O}_8$ ceramics, a small amount of Zr-substitution ($x = 0.2$) could significantly improve the $Q \times f$ values (from 19,852 to 44,048 GHz) and τ_f values (from 77.1 to -11.9 ppm/ $^\circ\text{C}$) of ceramics. Typically, $\text{ZnTi}_{0.8}\text{Zr}_{0.2}\text{Ta}_2\text{O}_8$ ($x = 0.2$) ceramics exhibited an excellent microwave dielectric property of $\epsilon_r \sim 29.9$, $Q \times f \sim 44,048$ GHz, and $\tau_f \sim -11.9$ ppm/ $^\circ\text{C}$ as the sintering temperature was 1300 $^\circ\text{C}$.

1 Introduction

With rapid development of mobile phone and modern wireless communication market, microwave dielectric materials, widely used in microwave components such as filters, wave guides resonators, duplexer, and antennas, are all significantly developed. This kind of materials needs to meet higher requirements: a medium dielectric constant (ϵ_r), a high-quality factor (Q), and a temperature frequency coefficient (τ_f) close to zero [1, 2].

Recently, tri-rutile structured $\text{ZnTiTa}_2\text{O}_8$ ceramics belonging to $\text{M}^{2+}\text{TiTa}_2\text{O}_8$ ($\text{M}^{2+} = \text{Zn, Mg, Co, Ni}$) system were reported to have microwave dielectric properties of $\epsilon_r \sim 46.2$, $Q \times f \sim 36,700$ GHz and $\tau_f \sim +74$ ppm/ $^\circ\text{C}$ [3–5]. However, the large τ_f value restricted the practical application of this ceramics, so how to adjust the τ_f value and improve the dielectric loss become more and more important for this kind of ceramics. Generally, there were three main methods to adjust the temperature coefficient of materials: (1) forming multiphase ceramics by using different structural ceramics with opposite τ_f value; (2) forming solid solution

by using ion substitution. (3) changing the inclination of oxygen octahedron through structural phase transformation. Compared with the other two methods, ion substitution was the most convenient and effective way to obtain temperature-stable ceramics without deteriorating other microwave properties (ϵ_r and $Q \times f$ value) [6]. Considering the radius of Zr^{4+} (0.72 Å) was closed to Ti^{4+} (0.605 Å), it was possible to form solid solution with a near-zero τ_f value by Zr^{4+} substitution for Ti^{4+} . For instance, Hsu et al. reported microwave dielectric properties of $\epsilon_r \sim 46$, high $Q \times f$ value $\sim 47,500$ GHz and $\tau_f \sim -9.5$ ppm/ $^\circ\text{C}$ were obtained for $\text{CaLa}_4(\text{Zr}_x\text{Ti}_{1-x})_4\text{O}_{15}$ ceramics with 0.05 wt% Zr substitution [7]. For $\text{CoTiNb}_2\text{O}_8$ ceramics, Y. Zhang et al. reported a near-zero τ_f of 4.4 ppm/ $^\circ\text{C}$ could be acquired by the substitution of Zr^{4+} to the Ti^{4+} position [6]. M.J. Wu et al. investigated $\text{Ni}_{0.5}(\text{Ti}_{0.5-x}\text{Zr}_x)\text{NbO}_4$ ceramics with τ_f value close to zero, which was obtained by adjusting the x value of 0.25–0.3 [8]. Moreover, Zr^{4+} substitution for Ti^{4+} could also effectively adjust the τ_f values without detrimental effect on $Q \times f$ values in the $\text{Zn}_{0.5}\text{Ti}_{1-x}\text{Zr}_x\text{NbO}_4$ system [9].

At present, there were few reports on the temperature coefficient regulation of $\text{ZnTiTa}_2\text{O}_8$ ceramics. Therefore, in this work, Zr^{4+} was chosen as a substitute ion to obtain microwave ceramics with stable temperature coefficient and excellent microwave dielectric properties. $\text{Zn}(\text{Ti}_{1-x}\text{Zr}_x)\text{Ta}_2\text{O}_8$ ($x = 0, 0.2, 0.4, 0.6, 0.8, 1$) ceramics were prepared via traditional solid reaction method. The sintering behavior,

✉ Yingchun Zhang
zycustb@163.com

¹ School of Materials Science and Engineering, University of Science and Technology Beijing, 100083 Beijing, People's Republic of China

crystal structure, Raman spectroscopy, microstructure, and microwave dielectric properties of the ceramics were studied.

2 Experimental procedure

A series of $\text{Zn}(\text{Ti}_{1-x}\text{Zr}_x)\text{Ta}_2\text{O}_8$ ($x = 0, 0.2, 0.4, 0.6, 0.8, 1$) ceramics samples were synthesized by conventional solid-state reaction route. Oxide powders of ZnO (99.9%), TiO_2 (99.9%), ZrO_2 (99.9%), and Ta_2O_5 (99.99%) were adopted as raw materials. Initially, according to the chemical ratio, the oxide materials was mixed with ethanol in polyethylene bottles and ball milled for 4 h. Subsequently, the slurries put into an alumina crucible were dried in a drying oven at 80 °C for 2 h, then sieved through 200 mesh and calcined at 1200 °C for 4 h with a heating rate of 5 °C/min. After milling and sieving again, the resultant powders were uniaxially compacted with 5 wt% polyvinyl alcohol into pellets under the pressure of 200 MPa. Finally, the green pellets were sintered at the temperature range of 1200–1350 °C for 4 h with a heating rate of 5 °C/min.

The relative densities of sintered samples were identified by Archimedes method. Crystal structure was undertaken by X-ray diffraction (XRD, Rigaku, DMAX-RB, Japan) with Cu $K\alpha$ radiation. Raman spectroscopy of these polished samples was acquired by a LabRam HR (Jobin-Yvon, France) excited with an Ar^+ laser (514.5 nm line). Microstructure of these ceramics samples was observed with scanning electron microscope (SEM, JSM-6480LV). Microwave dielectric properties of the ceramics were measured by a network analyzer (8720ES, Agilent, USA) using Hakki–Coleman's dielectric resonator method, modified and improved by Courtney and Kobayashi [10–12]. All measurements were taken in the frequency of 6–9 GHz at room temperature. The temperature coefficients of the resonant frequency (τ_f) were measured in the temperature ranging from 25 to 80 °C. The τ_f values were defined by the following relationship:

$$\tau_f = \frac{f_2 - f_1}{f_1(T_2 - T_1)}, \quad (1)$$

where f_1 and f_2 were the resonant frequency at T_1 and T_2 , respectively.

3 Results and discussion

3.1 Relative density

The sintering density of ceramics is one of the important factors which effect the microwave dielectric properties; therefore, the bulk density and relative density of

$\text{Zn}(\text{Ti}_{1-x}\text{Zr}_x)\text{Ta}_2\text{O}_8$ ceramics are evaluated and presented in Fig. 1. For each composition (Fig. 1a), the relative densities first increased and then decreased after reaching a maximum value along with the temperature enhancement. The bulk density of ceramics samples raised gradually from 6.92 to 7.43 g/cm^3 by increasing Zr^{4+} , which was attributed to the higher density of $\text{ZnZrTa}_2\text{O}_8$ (7.59 g/cm^3) than $\text{ZnTiTa}_2\text{O}_8$ (6.92 g/cm^3). Additionally, the optimum sintering temperature of samples where the maximum densities were acquired could be summarized. The measured relative density (Fig. 2b), ranged from 96.01 to 97.99%, which indicated that all samples sintered at their optimum temperature were well-sintered. Further, with the substitution of Zr^{4+} ($x = 0.2$), the relative density of samples sharply enhanced to 97.99%, which demonstrated that a small amount Zr^{4+} could improve the sinterability of ceramics.

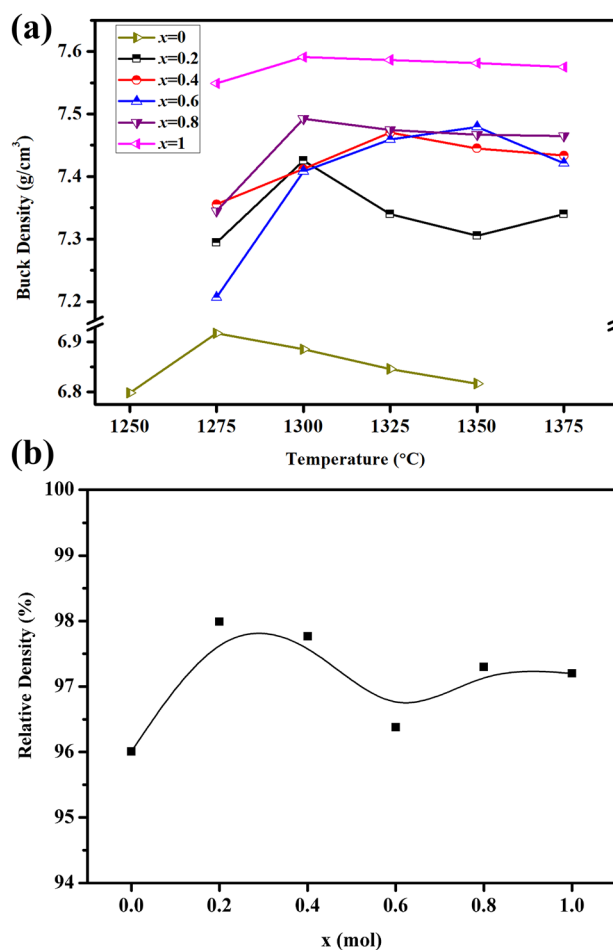
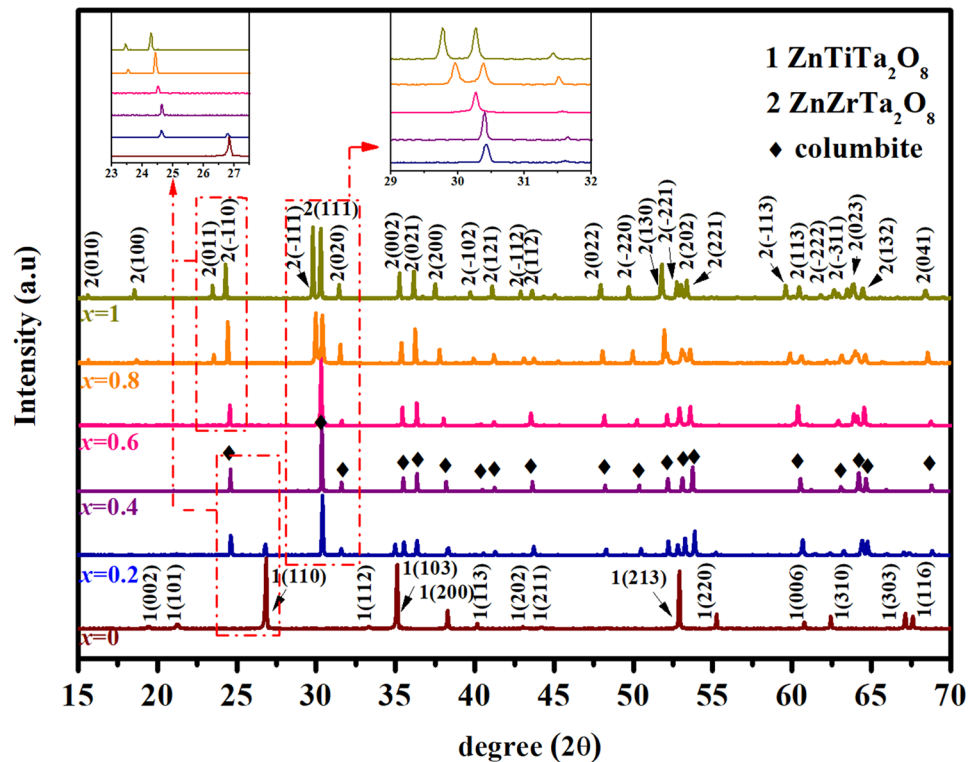


Fig. 1 **a** Bulk density and **b** relative density of $\text{Zn}(\text{Ti}_{1-x}\text{Zr}_x)\text{Ta}_2\text{O}_8$ ceramics ($x = 0$, at 1275 °C; $x = 0.2$, at 1300 °C; $x = 0.4$, at 1325 °C; $x = 0.6$, at 1350 °C; $x = 0.8$, at 1300 °C; $x = 0$, at 1300 °C)

Fig. 2 XRD pattern of $\text{Zn}(\text{Ti}_{1-x}\text{Zr}_x)\text{Ta}_2\text{O}_8$ ceramics sintered at their optimum temperature



3.2 Phase and structure

The XRD patterns of $\text{Zn}(\text{Ti}_{1-x}\text{Zr}_x)\text{Ta}_2\text{O}_8$ ceramics sintered at their optimum temperature are shown in Fig. 2. Through indexing the patterns, the ceramics adopted the tetragonal cell of the tri-rutile-type structure (JCPDS: #32-0702, $P4_2/mnm$ (#136)) when $x = 0$. However, when $x = 0.4-0.6$, all patterns were matched perfectly with the orthorhombic cell of columbite-type structure (JCPDS: #48-0326, $Pbcn$ (#60)). Finally, the monoclinic wolframite-type structure (JCPDS: #48-0324, $P2/c$ (#13)) could be observed in the compositions of $x = 0.8-1$. It is worth noting that the ceramics sample formed a mixture of tri-rutile and columbite structure with the nominal composition of $\text{ZnTi}_{0.8}\text{Zr}_{0.2}\text{Ta}_2\text{O}_8$ rather than a single phase as $x = 0.2$. As shown in the insets of Fig. 2, the (110) peak of tri-rutile structure disappeared gradually, the (111) and (110) peak position of columbite structure shifted to lower degree and some new diffraction peaks of monoclinic wolframite structure emerged during the process of structure evolution. This structural evolution in the $\text{Zn}(\text{Ti}_{1-x}\text{Zr}_x)\text{Ta}_2\text{O}_8$ ceramics system implied the non-negligible change of structure parameters as well as their properties.

The lattice parameters and cell volumes of $\text{Zn}(\text{Ti}_{1-x}\text{Zr}_x)\text{Ta}_2\text{O}_8$ ceramics are depicted in Fig. 3. From the results, it was found that there was a conspicuous variation on the cell volumes related to lattice parameters with Zr-substitution. Although a and b increased constantly with the increase of

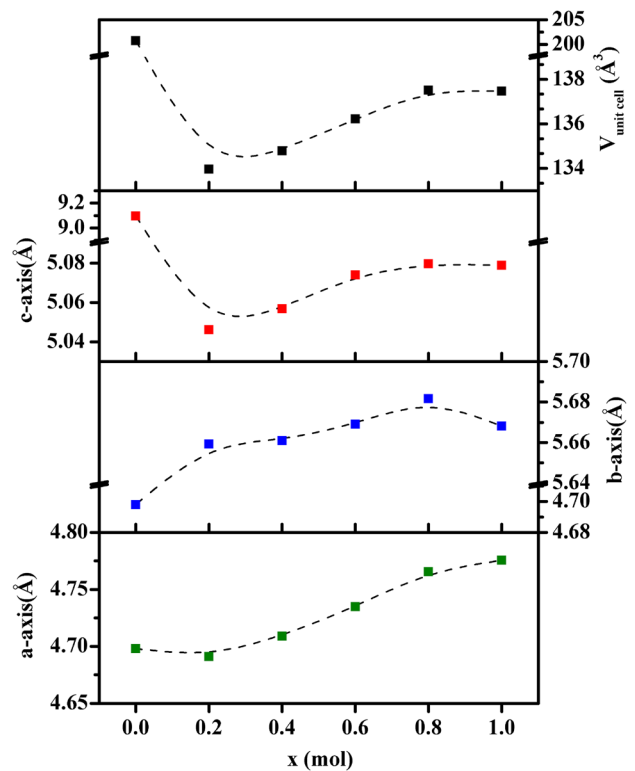


Fig. 3 Lattice parameters and cell volumes of $\text{Zn}(\text{Ti}_{1-x}\text{Zr}_x)\text{Ta}_2\text{O}_8$ ceramics

Zr⁴⁺ content, the *c* parameter, contributing most to the cell volume change in the compositions of $x = 0-1$, was responsible for the shrinkage of cell volume. Afterwards, the lattice parameters (both *a*, *b* and *c*) showed an upward trend. Therefore, the variation trend of cell volumes was similar to that of *c*. In addition, Fig. 4 shows the structural schematic diagrams of ZnTiTa₂O₈, ZnZrTa₂O₈ and Zn(Ti_{1-x}Zr_x)Ta₂O₈ ceramics ($0.4 \leq x \leq 0.6$). For tri-rutile structured ZnTiTa₂O₈ ceramics (Fig. 4a), Zn²⁺, Ti⁴⁺ and Ta⁵⁺ were all divided into two types of cations (Zn1, Zn2, Ti1, Ti2, Ta1 and Ta2), respectively. The 2e Wyckoff position was distributed by Zn1(0.4)/Ti1(0.4)/Ta1(0.2) cations while Zn2(0.175)/Ti2(0.175)/Ta2(0.650) cations occupied the 4e Wyckoff position, whereas oxygen anions were located in 4f and 8j Wyckoff positions [5]. For monoclinic wolframite structured ZnZrTa₂O₈ ceramics (Fig. 4b), the 2e Wyckoff position was distributed by Zn/Zr cations, Ta cations occupied the 2f Wyckoff position and oxygen anions were located in 4g Wyckoff position [1]. As for columbite structure (Fig. 4c), Zn/Zr/Ti cations occupied the 4c Wyckoff

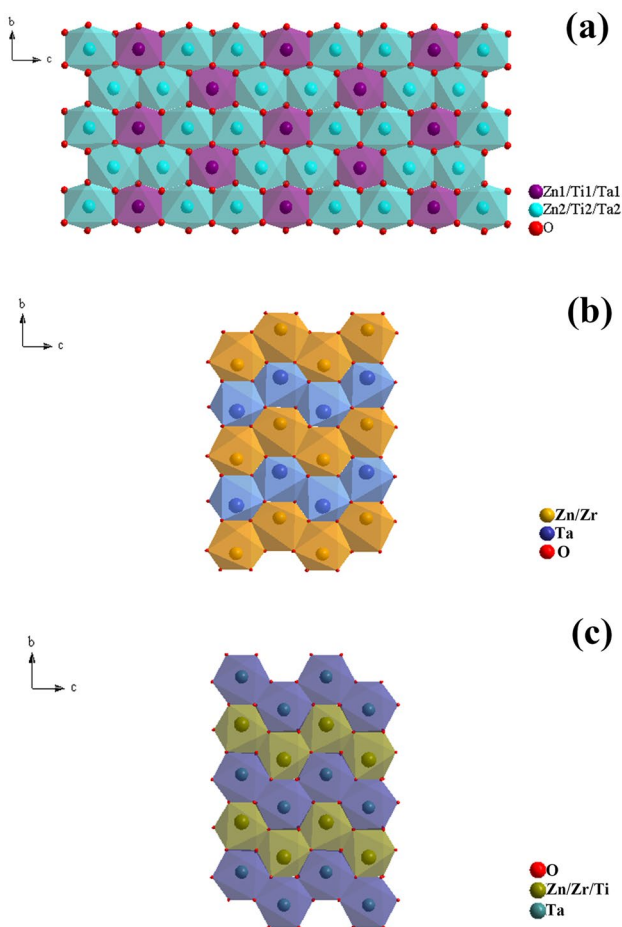


Fig. 4 Structural schematic diagrams of **a** ZnTiTa₂O₈ ceramics, **b** ZnZrTa₂O₈ ceramics and **c** Zn(Ti_{1-x}Zr_x)Ta₂O₈ ceramics ($0.4 \leq x \leq 0.6$)

position, while Ta cations and O anions occupied the 8*d* Wyckoff position. Obviously, the number of oxygen octahedrons of ZnTiTa₂O₈ was almost twice as that of ZnZrTa₂O₈ or Zn(Ti_{1-x}Zr_x)Ta₂O₈ ($0.4 \leq x \leq 0.6$) along the direction of *c*-axis. In other words, the lattice parameter along *c*-axis was absolutely distinct between them. This result was corroborated in Fig. 3. In short, the structural evolution in the Zn(Ti_{1-x}Zr_x)Ta₂O₈ ceramics would have a strong influence on microwave dielectric properties.

3.3 Raman spectroscopy

In order to characterize the phase composition of Zn(Ti_{1-x}Zr_x)Ta₂O₈ ceramics, Raman spectroscopy which was sensitive to the variation of structure was employed. Figure 5 displays the Raman spectra of Zn(Ti_{1-x}Zr_x)Ta₂O₈ ceramics over the frequency range 50–1000 cm⁻¹. Three types of Raman spectra could be clearly observed, which demonstrated that there were three different structures existing in the Zn(Ti_{1-x}Zr_x)Ta₂O₈ ceramics system, which was in coincidence with the XRD results. In fact, only few Raman peaks were depicted in Fig. 5 because some weak vibration modes could be overlapped or broadened [6]. Tri-rutile structured ZnTiTa₂O₈ ceramics had four strongest Raman peaks, including B_{1g} mode (72 cm⁻¹) caused by the rotating of [TaO₆] oxygen octahedrons, E_g mode (386 cm⁻¹) originated from the vibration of cations and rotation of oxygen octahedrons, E_g mode (457 cm⁻¹) ascribed to the stretching vibration of Ti–O bond and A_{1g} mode (697 cm⁻¹) resulted from the stretching of Ta–O bond [13]. These modes were only detected from the pure phase of ZnTiTa₂O₈ ceramics. However, with a small amount of Zr-substitution ($x = 0.2$), it displayed quite difference type of vibration modes belonging to columbite structure, indicating that the main structure of

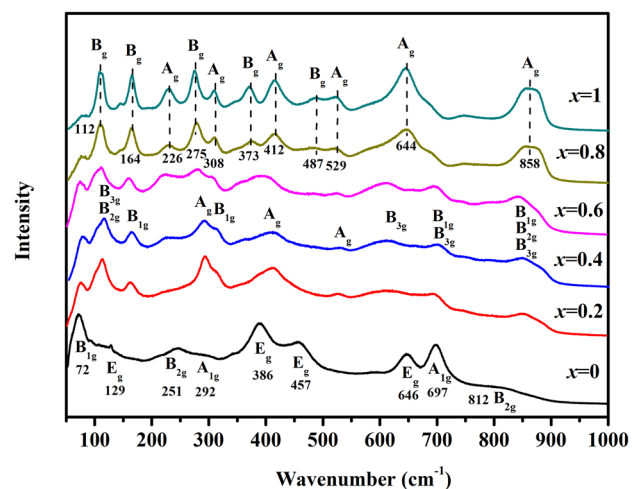


Fig. 5 Raman spectra of Zn(Ti_{1-x}Zr_x)Ta₂O₈ ceramics over the frequency range 50–1000 cm⁻¹

the samples had changed at this composition. When transition took place from tri-rutile to columbite, the E_g mode (386 cm^{-1}) and A_{1g} mode (697 cm^{-1}) belonging to the tri-rutile structure disappeared and the main peaks of columbite structure B_{2g} (110 cm^{-1}), B_{1g} (171 cm^{-1}), A_g (293 cm^{-1}) emerged [14]. These modes were observed plainly from $x = 0.2$ to $x = 0.6$. Starting with $x = 0.8$, four basic modes appeared which were summarized of B_g mode (122 cm^{-1}) caused by lattice vibration, B_g mode (275 cm^{-1}) resulted from the stretching vibration of Zn–O bond, A_g mode (644 cm^{-1}) caused by Ta–O stretching vibration. Meanwhile, the mode at 858 cm^{-1} originated from Zr–O symmetric vibration also was a prominent peak [6, 15]. Beyond that, it could also be observed that the Raman spectra peak of monoclinic wolframite structure gradually intensified along with increase of Zr^{4+} . The variation of Raman spectra was

consistent with XRD analysis shown in Fig. 2. It demonstrated that the overall structural evolution process was from tri-rutile to coexistence of tri-rutile and columbite, then to columbite and finally to monoclinic wolframite structure.

3.4 Morphological

The SEM images of $Zn(Ti_{1-x}Zr_x)Ta_2O_8$ ceramics sintered at different temperatures are given in Fig. 6. The EDS analysis of points marked in Fig. 6 are listed in the Table 1. The ceramics exhibited a dense microstructure with grain size of 2–15 μm . For $x = 0$ (Fig. 6a), pure phase of $ZnTiTa_2O_8$ ceramic depicted a uniform distribution of 13–15 μm grain size. Whereas for $x = 0.2$ (Fig. 6b), evidently, the grain with different morphologies could be observed, and marked as B and C, respectively. EDS results illustrated the specimen

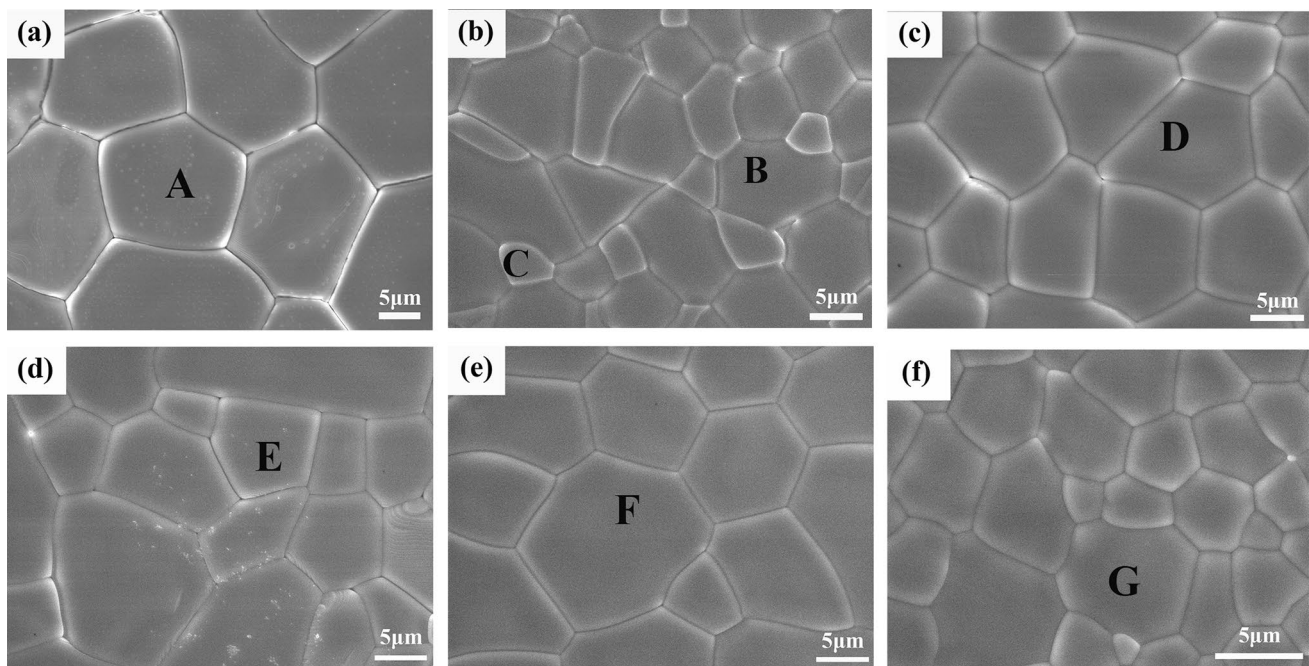


Fig. 6 SEM images of $Zn(Ti_{1-x}Zr_x)Ta_2O_8$ ceramics sintered at different temperatures for 4 h: **a** $x = 0$, at $1250\text{ }^\circ\text{C}$; **b** $x = 0.2$, at $1250\text{ }^\circ\text{C}$; **c** $x = 0.4$, at $1300\text{ }^\circ\text{C}$; **d** $x = 0.6$, at $1300\text{ }^\circ\text{C}$; **e** $x = 0.8$, $1350\text{ }^\circ\text{C}$; and **f** $x = 1$, at $1400\text{ }^\circ\text{C}$

Table 1 EDS analysis of points marked on Fig. 6

Atom (%)	A $x = 0$	B $x = 0.2$	C $x = 0.2$	D $x = 0.4$	E $x = 0.6$	F $x = 0.8$	G $x = 1$
Zn	6.90	7.84	7.33	8.60	8.07	6.52	7.78
Ti	6.54	6.19	6.74	4.45	3.25	1.24	–
Zr	–	1.41	–	4.36	5.60	5.52	7.04
Ta	15.37	14.85	15.47	14.81	13.80	12.27	17.75
O	58.40	57.90	58.85	55.33	55.39	57.81	55.49
C	12.79	11.81	11.61	12.45	13.89	16.64	11.94
Total	100	100	100	100	100	100	100

formed a mixture phase of $\text{ZnTiTa}_2\text{O}_8$ and $\text{ZnTi}_{0.8}\text{Zr}_{0.2}\text{Ta}_2\text{O}_8$, which was consistent with XRD analysis. At $0.4 \leq x \leq 0.8$, all the grains of the ceramic samples presented a polygonal morphology with grain size of 5–10 μm . As x increased to 1, the grains were compactly accumulated and the grain size (2–5 μm) decreased obviously. It means that the average grain size of pure phase of $\text{ZnZrTa}_2\text{O}_8$ ceramic was smaller than that of $\text{ZnTiTa}_2\text{O}_8$ ceramics.

3.5 Microwave dielectric properties

Dielectric constant of $\text{Zn}(\text{Ti}_{1-x}\text{Zr}_x)\text{Ta}_2\text{O}_8$ ceramics are provided in Fig. 7. The dielectric constants of all compositions enhanced with the temperature increasing and then declined after almost reaching the maximum value at their optimum densification temperature, which shared a similar trend with densities. It was easy to accept that relative density had a

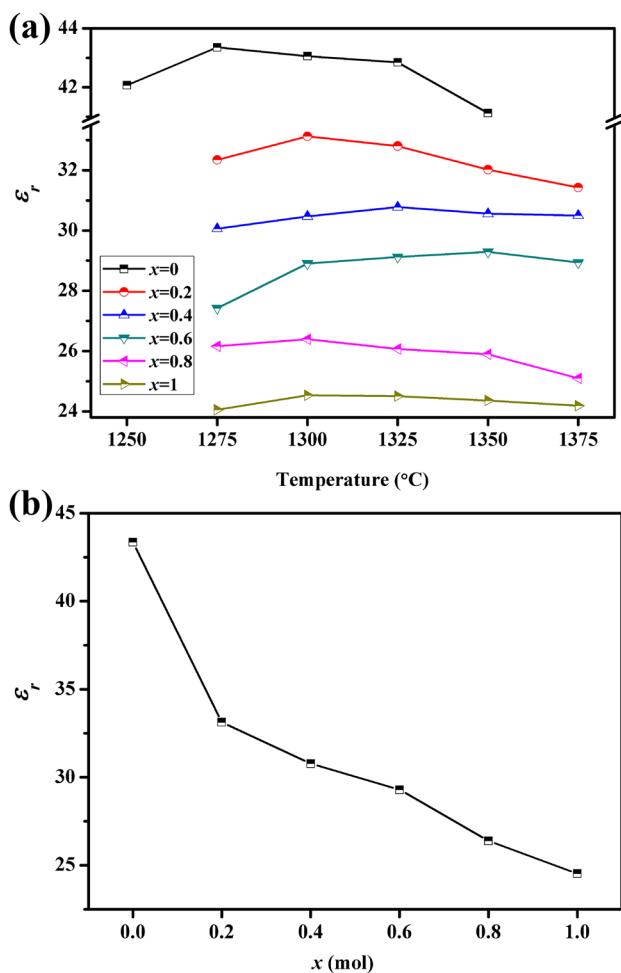


Fig. 7 **a** Dielectric constant of $\text{Zn}(\text{Ti}_{1-x}\text{Zr}_x)\text{Ta}_2\text{O}_8$ ceramics as a function of sintering temperature; **b** the variety of dielectric constant of $\text{Zn}(\text{Ti}_{1-x}\text{Zr}_x)\text{Ta}_2\text{O}_8$ ceramics versus Zr-substitution ($x = 0$, at 1275 $^\circ\text{C}$; $x = 0.2$, at 1300 $^\circ\text{C}$; $x = 0.4$, at 1325 $^\circ\text{C}$; $x = 0.6$, at 1350 $^\circ\text{C}$; $x = 0.8$, at 1300 $^\circ\text{C}$; $x = 0$, at 1300 $^\circ\text{C}$)

strong effect on the dielectric constants [16, 17]. For samples with different composition (Fig. 7b), it could be evidently observed that the dielectric constant declined sharply in pace with the increase of Zr^{4+} content. For samples with Zr^{4+} free, the dielectric constant showed the maximum value of 43.35 which followed similar value as Park et al. reported [3]. For a minor Zr-substitution ($x = 0.2$), the dielectric constant dropped precipitously to 33.12, which was attributed to the structural transition of ceramics. In this composition, although the tri-rutile and columbite structures coexisted, the latter had assumed a dominant role. Generally, most columbite structured oxides possessed lower dielectric constant (17–25) [18–20]; thus, the dielectric constant decreased with the columbite structured ceramics formation. Upon further increasing Zr^{4+} , the dielectric constant continued to decline. When Zr^{4+} completely replaced Ti^{4+} ($x = 1$), monoclinic wolframite structured $\text{ZnZrTa}_2\text{O}_8$ was formed and showed a lower dielectric constant of 24.53. In this work, the dielectric constant of $\text{Zn}(\text{Ti}_{1-x}\text{Zr}_x)\text{Ta}_2\text{O}_8$ ceramics declined gradually with increasing Zr^{4+} content. This phenomenon was contrary to the ionic dielectric polarizability analysis which dielectric constant should increase with the enhancement of Zr^{4+} content due to the higher ionic dielectric polarizability of Zr^{4+} (3.25 \AA) than Ti^{4+} (2.93 \AA) [6]. This deviation was mainly ascribed the dominant and decisive influence of structural evolution on the properties of ceramics.

Figure 8 displays the $Q \times f$ values of $\text{Zn}(\text{Ti}_{1-x}\text{Zr}_x)\text{Ta}_2\text{O}_8$ ceramics. For the samples with same composition, when $x \leq 0.2$ (Fig. 8a), the variation trend of $Q \times f$ values was similar with that of density. However, when $x \geq 0.4$ (Fig. 8b), $Q \times f$ values kept increasing as the rise of temperature, which mainly caused by the abnormal growth of grains at higher temperature. The total number of grain boundaries in ceramics decreased with grain size increasing. The defects caused by grain boundaries, such as pores, vacancies, and impurities also declined, thus reducing the extrinsic dielectric loss and showing higher $Q \times f$ values [21, 22]. For the samples with different Zr-substitution, it is obvious from Fig. 8b that $Q \times f$ values changed dramatically at two component points, which was $x = 0.2$ and $x = 0.8$, respectively. The main reason for this phenomenon was that there had been marked structural transitions at these two components. The maximum $Q \times f$ values of 44,048 GHz could be achieved at the compositions of $x = 0.2$.

Figure 9 exhibits the τ_f values of $\text{Zn}(\text{Ti}_{1-x}\text{Zr}_x)\text{Ta}_2\text{O}_8$ ceramics. It was well recognized that the temperature coefficients of the resonance frequency of $\text{Zn}(\text{Ti}_{1-x}\text{Zr}_x)\text{Ta}_2\text{O}_8$ ceramics declined gradually, and could gain the closest value to zero at the compositions of $x = 0.2$. For samples with Zr^{4+} free, the τ_f values reached 77.1 $\text{ppm}/^\circ\text{C}$, and for a minor Zr-substitution ($x = 0.2$), the τ_f values sharply declined to $-11.9 \text{ ppm}/^\circ\text{C}$. Finally, when Zr^{4+} completely

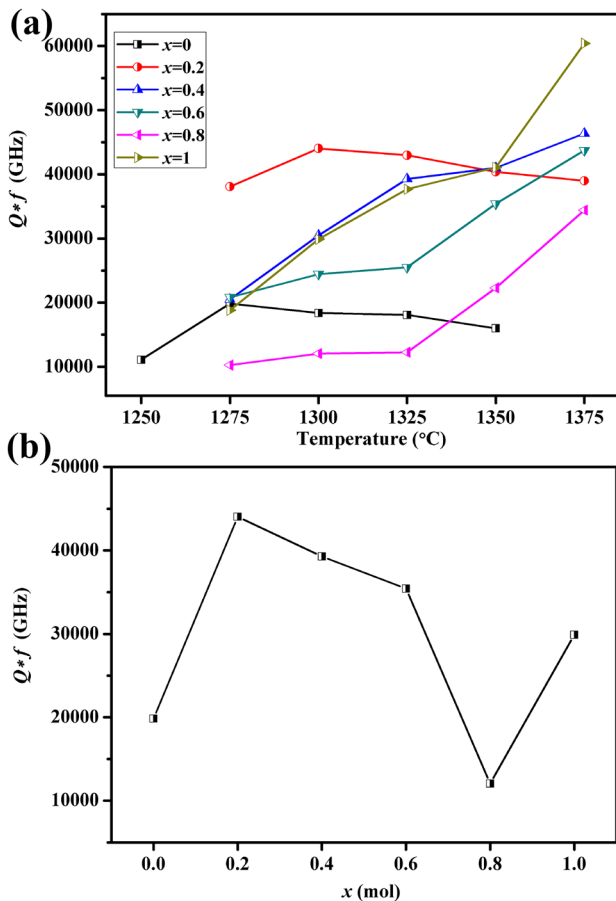


Fig. 8 **a** $Q \times f$ values of $\text{Zn}(\text{Ti}_{1-x}\text{Zr}_x)\text{Ta}_2\text{O}_8$ ceramics as a function of sintering temperature; **b** the variety of $Q \times f$ values of $\text{Zn}(\text{Ti}_{1-x}\text{Zr}_x)\text{Ta}_2\text{O}_8$ ceramics versus Zr-substitution ($x = 0$, at 1275 °C; $x = 0.2$, at 1300 °C; $x = 0.4$, at 1325 °C; $x = 0.6$, at 1350 °C; $x = 0.8$, at 1300 °C; $x = 0$, at 1300 °C)

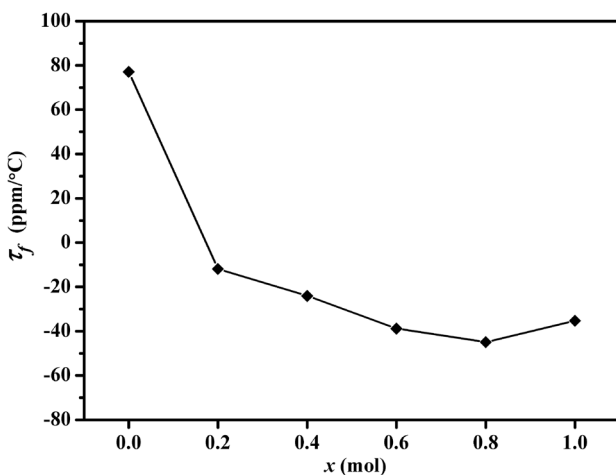


Fig. 9 The variety of τ_f values of $\text{Zn}(\text{Ti}_{1-x}\text{Zr}_x)\text{Ta}_2\text{O}_8$ ceramics versus Zr-substitution ($x = 0$, at 1275 °C; $x = 0.2$, at 1300 °C; $x = 0.4$, at 1325 °C; $x = 0.6$, at 1350 °C; $x = 0.8$, at 1300 °C; $x = 0$, at 1300 °C)

replaced Ti^{4+} ($x = 1$), the τ_f value of samples was -35.22 ppm/°C. Generally, τ_f value was related to the microstructure, composition, and structure of the materials [23]. In order to reveal the relationship between τ_f values and the structure of ceramics, the microwave dielectric properties of ceramics with tri-rutile, columbite, and wolframite structures are summarized in Table 2. Referring to the published literatures, most tri-rutile structured ceramics had positive τ_f values (74–111.54 ppm/°C), while ceramics with columbite and wolframite structure exhibited negative τ_f values (-38 to -56.54 , -24.96 to -32 ppm/°C, respectively). Herein, τ_f values of these three pure phase ceramics were basically consistent with the results in Table 2. As for samples with the coexistence of tri-rutile and columbite structure ($x = 0.2$), τ_f value was adjusted to -11.9 ppm/°C due to the composite of two phases. The τ_f values of composites could be calculated by the following mixing rule [27, 28]:

$$\tau_f = v_1 \tau_{f1} + v_2 \tau_{f2}, \quad (2)$$

where τ_f was the temperature coefficient of resonant frequency of composite ceramics. τ_{f1} and τ_{f2} were the temperature coefficient of resonant frequency of two different phases of ceramics. v_1 and v_2 were the volume fraction of the two phases, respectively. According to the XRD results, the volume fraction of columbite phase ($\sim 83.8\%$) in ceramics was larger than that of tri-rutile phase ($\sim 16.2\%$) when $x = 0.2$. Therefore, it could be estimated that the τ_f value should be a negative value closing to 0. All in all, in this work, the τ_f values were significantly affected by structural transition in $\text{Zn}(\text{Ti}_{1-x}\text{Zr}_x)\text{Ta}_2\text{O}_8$ ceramics.

4 Conclusions

In this work, the sintering behavior, crystal structure, Raman spectroscopy, microstructure, and microwave dielectric properties of $\text{Zn}(\text{Ti}_{1-x}\text{Zr}_x)\text{Ta}_2\text{O}_8$ ($x = 0-1$) ceramics were studied. It was found that there were three structure types (tri-rutile, columbite, and monoclinic wolframite) existing in the $\text{Zn}(\text{Ti}_{1-x}\text{Zr}_x)\text{Ta}_2\text{O}_8$ ceramics system. For samples with Zr^{4+} free ($x = 0$, $\text{ZnTiTa}_2\text{O}_8$), they possessed the tri-rutile-type structure. When $0.4 \leq x \leq 0.6$, a columbite-type structure was detected. For $x \geq 0.8$, all samples remained monoclinic wolframite-type structure. However, a mixture of tri-rutile and columbite structure was observed when $x = 0.2$. The structural evolution process was from tri-rutile to coexistence of tri-rutile and columbite, then to columbite and finally to monoclinic wolframite structure with the increase of Zr^{4+} content. The variation of ϵ_r , improvement of $Q \times f$ values and betterment of τ_f values of $\text{Zn}(\text{Ti}_{1-x}\text{Zr}_x)\text{Ta}_2\text{O}_8$ ceramics were influenced strongly by the structural transition. Typically, $\text{ZnTi}_{0.8}\text{Zr}_{0.2}\text{Ta}_2\text{O}_8$ ($x = 0.2$) ceramics

Table 2 Microwave dielectric properties of ceramics with tri-rutile, columbite and wolframite structure

Materials	Crystal structure	T_s (°C)	ϵ_r	$Q \times f$ (GHz)	τ_f (ppm/°C)	Ref.
NiTiTa ₂ O ₈	Tri-rutile	1350	39.86	25,051	75	[24]
ZnTiTa ₂ O ₈	Tri-rutile	1250	46.2	36,700	74.00	[3]
Co _{0.5} Ti _{0.5} TaO ₄	Tri-rutile	1075	40.69	17,291	114.54	[17]
ZnNb ₂ O ₆	Columbite	1150	25.0	83,700	− 56.00	[22]
NiNb ₂ O ₆	Columbite	1150	22.6	40,100	− 38.00	[22]
CoNb ₂ O ₆	Columbite	1100	22.8	11,300	− 44.70	[22]
NiZrNb ₂ O ₈	Wolframite	1100	29.31	22,985	− 24.96	[25]
ZnZrTa ₂ O ₈	Wolframite	1320	32	110,700	− 32.00	[1]
MnZrNb ₂ O ₈	Wolframite	1400	16.7	40,700	− 29.6	[26]

exhibited excellent microwave dielectric properties of $\epsilon_r \sim 29.9$, $Q \times f \sim 44,048$ GHz, and $\tau_f \sim -11.9$ ppm/°C at $T_s = 1300$ °C.

Acknowledgements This work has been financially supported by the National Natural Science Foundation of China (No. 51772022) and Fundamental Research Funds for the Central Universities (FRF-GF-18-005A).

References

- X.S. Lyu, L.X. Li, S. Zhang, H. Sun, S. Li, J. Ye, B.W. Zhang, J.T. Li, *J. Eur. Ceram. Soc.* **36**, 931–935 (2016)
- M.J. Wu, Y.C. Zhang, M.Q. Xiang, *J. Mater. Sci. Mater. Electron.* **29**, 14471–14478 (2018)
- J.H. Park, Y.J. Choi, S. Nahm, J.G. Park, *J. Alloys Compd.* **509**, 6908–6912 (2011)
- N. Kumada, N. Koike, K. Nakanome, S. Yanagida, T. Takei, A. Miura, E. Magome, C. Moriyoshi, Y. Kuroiwa, *J. Asian Ceram. Soc.* **5**, 284–289 (2017)
- N. Kumada, N. Koike, K. Nakanome, S. Yanagida, T. Takei, A. Miura, E. Magome, C. Moriyoshi, Y. Kuroiwa, *J. Asian Ceram. Soc.* **6**, 247–253 (2018)
- Y. Zhang, Y.C. Zhang, M.Q. Xiang, *J. Eur. Ceram. Soc.* **36**, 1945–1951 (2016)
- C.H. Hsu, C.J. Huang, *J. Alloys Compd.* **587**, 45–49 (2014)
- M.J. Wu, J.D. Chen, Y.C. Zhang, *Funct. Mater. Lett.* **12**, 1950020–1950023 (2019)
- Q.W. Liao, L.X. Li, X. Ding, *Solid State Sci.* **14**, 1385–1391 (2012)
- B.W. Hakki, P.D. Coleman, *IRE Trans. Microw. Theory* **8**, 402–410 (1960)
- W.E. Courtney, *IEEE Trans. Microw. Theory* **18**, 476–485 (1970)
- Y. Kobayashiy, M. Katoh, *IEEE Trans. Microw. Theory* **33**, 586–592 (1985)
- H.Y. Yang, S.R. Zhang, Y.W. Chen, H.C. Yang, Y. Yuan, E.Z. Li, *Inorg. Chem.* **58**, 968–976 (2019)
- D.P. Xu, Y. Liu, Q. Zhou, T. Cui, H. Yuan, W. Wang, Z. Shi, L. Li, *J. Alloys Compd.* **618**, 694–699 (2015)
- H.T. Wu, Z.B. Feng, Q.J. Mei, J.D. Guo, J.X. Bi, *J. Alloys Compd.* **648**, 368–373 (2015)
- C.F. Tseng, *J. Eur. Ceram. Soc.* **34**, 3641–3648 (2014)
- C.F. Tseng, *J. Eur. Ceram. Soc.* **35**, 383–387 (2015)
- R.C. Pullar, J.D. Breeze, N.M. Alford, *J. Am. Ceram. Soc.* **88**, 2466–2471 (2005)
- Y.C. Liou, C.Y. Shiue, M.H. Weng, *J. Eur. Ceram. Soc.* **29**, 1165–1171 (2009)
- H.J. Lee, I.T. Kim, K.S. Hong, *Jpn. J. Appl. Phys.* **36**, 1318–1320 (1997)
- Y. Zhang, Y.C. Zhang, *J. Alloys Compd.* **683**, 86–91 (2016)
- N. Ichinose, T. Shimada, *J. Eur. Ceram. Soc.* **26**, 1755–1759 (2006)
- Y.C. Chen, Y.W. Zeng, *J. Alloys Compd.* **481**, 369–372 (2009)
- S.Y. Wang, J.D. Chen, Y.J. Zhang, Y.C. Zhang, *J. Alloys Compd.* **805**, 852–858 (2019)
- M.J. Wu, Y.C. Zhang, J.D. Chen, M.Q. Xiang, *J. Alloys Compd.* **747**, 394–400 (2018)
- S.D. Ramarao, V.R.K. Murthy, *Scr. Mater.* **69**, 274–277 (2013)
- C.L. Huang, M.H. Weng, *Mater. Res. Bull.* **36**, 2741–2750 (2001)
- Y. Lv, R.Z. Zuo, Y. Cheng, C. Zhang, *J. Am. Ceram. Soc.* **96**, 3862–3867 (2013)

Publisher's Note Springer Nature remains neutral with regard to jurisdictional claims in published maps and institutional affiliations.